nature physics

SUPPLEMENTARY INFORMATION

DOI: 10.1038/NPHYS3339

Measurement of the mobility edge for 3D Anderson localization

G. Semeghini,[1] M. Landini,[1,2] P. Castilho,[1] S. Roy,[1] G. Spagnolli,[1,2]
A. Trenkwalder,[1,2] M. Fattori,[1,2] M. Inguscio,[1,3] and G. Modugno[1,2]

[1] *LENS and Dipartimento di Fisica e Astronomia, Universitá di Firenze, Via N. Carrara 1, 50019, Sesto Fiorentino, Italy*
[2] *CNR-INO, Via N. Carrara 1, 50019, Sesto Fiorentino, Italy*
[3] *INRIM, Strada delle Cacce 91, 10135, Torino, Italy*

1. SYSTEM GEOMETRY AND PREPARATION

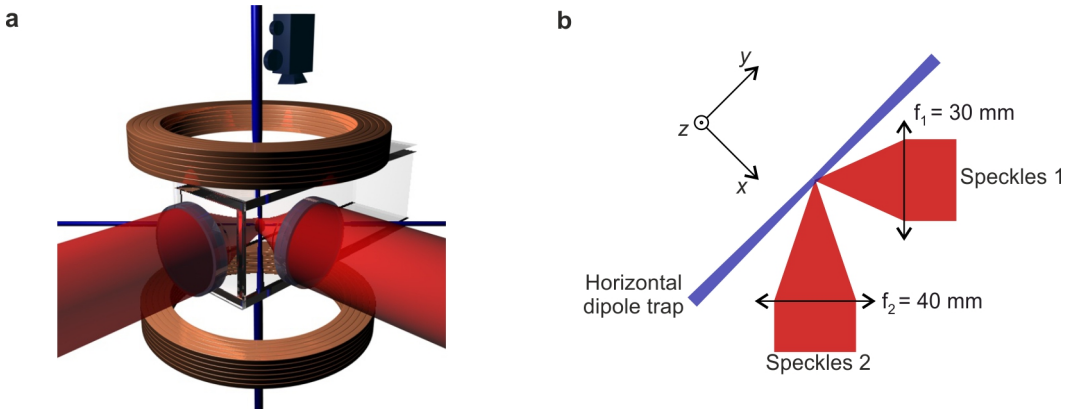

FIG. S1.

The dipole trap we initially use to prepare the Bose-Einstein condensate is the result of two crossed 1064-nm laser beams (blue in **a**,**b**), providing trap frequencies of 110 Hz along x and z and 25 Hz along y. The disordered potential is created by the interference of two focused speckle beams, intersecting at 90° at the atoms position (red). The speckle wavelength is λ=762 nm, blue-detuned with respect to the ^{39}K optical transitions (767 nm and 770 nm). We use two pairs of coils to tune the scattering length a via a magnetic Feshbach resonance and to compensate gravity (for more details, see [1]). We have two imaging systems available: one along the z axis and the other one along the same direction of the speckles 1 (see Fig.S1**b**). This allows us to study the expansion dynamics of the cloud along all the three main axes. We normally use the imaging along z sketched here, since we are especially interested in the dynamics along x.

In addition to the disordered speckle potential, the atoms are subjected to a weak additional optical and magnetic potential. We indeed use a vertically-oriented homogeneous magnetic field to control the interaction, while a magnetic field gradient compensates gravity. The two sets of magnetic field coils generate weak curvatures, which we partially compensate with a weakly focused laser beam in the vertical direction. The first non-negligible terms of the resulting potential around the initial position of the atoms are $V_{res}(x,y,z) \simeq \frac{1}{2}m(-(2\pi \times 3.22 \text{ Hz})^2 z^2 + (2\pi \times 11 \text{ Hz})^2 y^2 - (12 \text{ Hz}^2/\mu\text{m})x^3)$. Here the axes are the same as in Fig.S1. The anti-trapping curvature along z is caused by a non-perfect Helmoltz configuration of the Feshbach coils. In the x direction an off-center dipole trap cancels a magnetic field gradient along the same direction. The resulting potential has a cubic spatial dependence, flat around the atoms position to allow for a free expansion in the disorder. In the y direction the same optical trap contributes to a weak trapping potential. By noticing that the typical energy scale for the system is of several tens on nK, we could define a spatial region in which the spurious fields stay below $\simeq$5 nK, so that if the system remains within this region, we can consider negligible the effect of the residual curvatures. The size of the region amounts to 144 μm along z, 42 μm along y and 112 μm along x. In the fast diffusive regime (very small V_R), we indeed observe some deviations from the expected expansion when the cloud size approaches the region's boundaries. We expect that the effect of such a

DOI: 10.1038/NPHYS3339

background potential is minimal at the mobility edge, where the typical energies we explore in this work range from 20 nK to 100 nK. Note also that the potential corresponds to antitrapping in two directions, and to trapping in the third direction, suggesting that the net effect on the 3D problem is less than that in the individual directions.

2. CHARACTERIZATION OF THE DISORDERED POTENTIAL

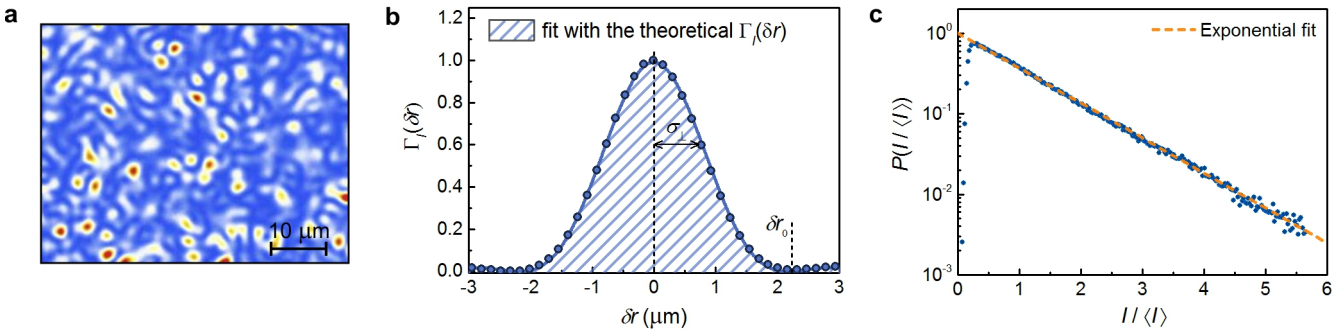

FIG. S2.

We image ex-situ the two speckle beams at their focus position with a CCD camera and we measure the waists of the Gaussian envelopes (s_1=1280(10) μm and s_2=1315(10) μm). **a**) Using a 35x microscope we can detect the fine structure of the speckles. From these images we can derive the intensity autocorrelation function $\Gamma_I(\delta r)$ reported in (**b**), which is well fitted by the theoretical Bessel function profile (see [2]). The transverse correlation length is given by $\sigma_\perp = \delta r_0/\pi$, where δr_0 is the position of the first zero. We measure $\sigma_{\perp 1}$=0.73(5) μm and $\sigma_{\perp 2}$=0.80(6) μm. **c**) For each speckles we also derive the intensity distribution function $P(I)$. We find that it decays exponentially according to $P(I) = 1/\langle I\rangle \exp(-I/\langle I\rangle)$, as expected for fully developed speckles [2]. The deviation at low I is due to the finite resolution of the imaging system used to calibrate the speckles.

We then use these measurements on the two speckle beams to reconstruct the properties of the final 3D potential. When the beams cross at 90° and the interference pattern adds to the speckle modulation, the main axes of the problem are the ones in Fig.S1. In the y direction, interference fringes split the speckles into smaller substructures and the first zero in the correlation function δr_0 is given by half the distance between two interference maxima, so that $\sigma_{Ry} = \lambda/(2\sqrt{2}\pi)$=0.09 μm. Along z we calculate the average between the transverse correlation lengths of the two speckles $\sigma_{Rz} = (\sigma_{\perp 1} + \sigma_{\perp 2})/2$=0.76 μm, while σ_{Rx} is the projection at 45° of the same average: $\sigma_{Rx} = \sigma_{Rz}\sqrt{2}$=1.08 μm. From the geometric average on the three directions we get σ_R=0.41 μm.

As for the intensity distribution $P(I)$, the field generated by two interfering speckles is predicted to preserve the same exponential distribution of the single speckles with $\langle I_{tot}\rangle = \langle I_1\rangle + \langle I_2\rangle$ (see [2]). An angle $\Delta\theta$ between the polarizations of the two speckles would reduce the contrast in the interference and hence modify $P(I)$ at low I. Considering the geometry of our experimental setup, we estimate $\Delta\theta \leq 5°$. For small $\Delta\theta$, the position of the maximum in $P(I)$ is expected to move to $\Delta\theta^2/4\ln(4/\Delta\theta^2)\langle I_{tot}\rangle$, which in our case corresponds to $\approx 0.01\langle I_{tot}\rangle$. Such a small modification is not expected to affect the localization properties of the system, since the typical energies in the experiment range from $V_R/2$ to V_R, hence far from this low I region.

All measurements have been averaged over different realization of the disorder. To change the speckle pattern, we rotate one of the diffusive plates in steps of approximately 20°.

3. CALIBRATION OF THE DISORDER AMPLITUDE

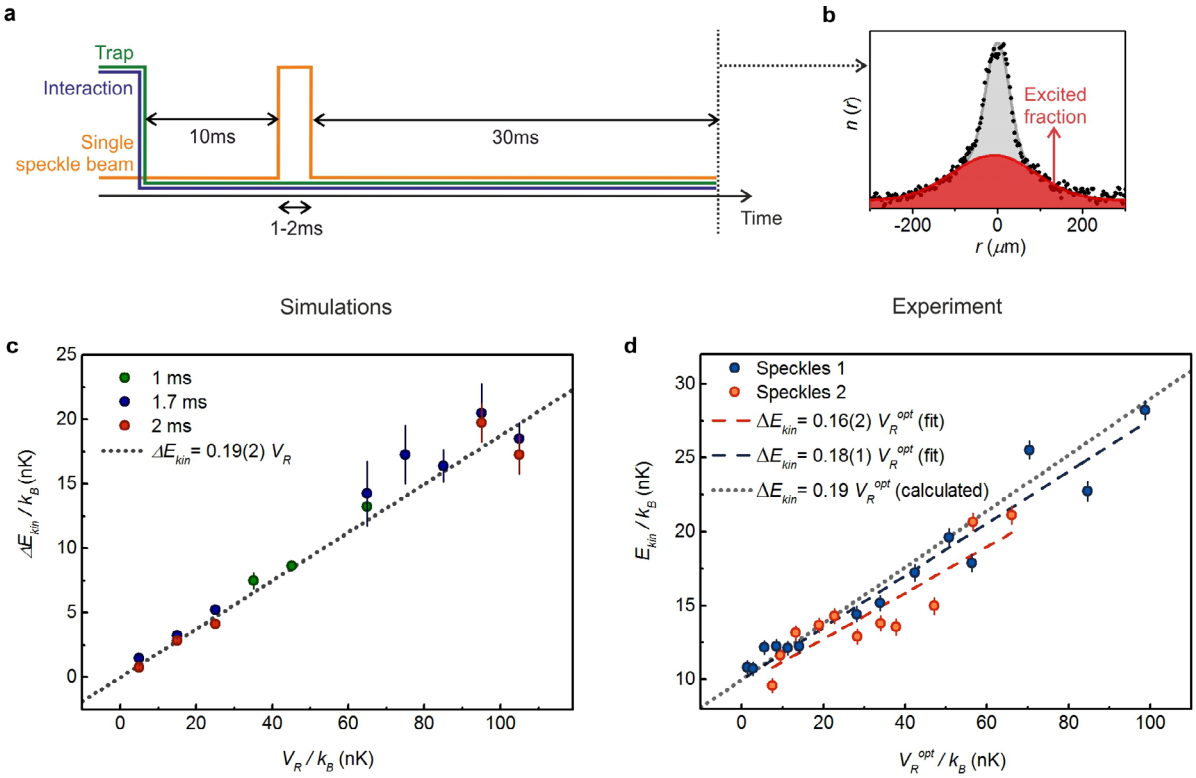

FIG. S3.

V_R is calibrated using two different methods. First, we compute a V_R^{opt} from the light intensity of the speckles, obtained by measuring ex-situ the spatial envelope of the individual speckle beams and their total optical power. For this optical calibration we estimate a relative uncertainty of 10%. Second, we perform an in-situ calibration from the dynamics of the atoms. Since our 3D disorder is the superposition of two separate speckle patterns, we calibrate them independently. **a**) We apply a short pulse of the speckle potential to a non-interacting condensate in free expansion, and we measure its final momentum distribution. Using a single speckle beam at a time, the problem is effectively 2D, being the longitudinal correlation length much longer than the atomic displacement on the short-time scale we consider ($\sigma_{\parallel} \simeq 10\sigma_{\perp}$). **b**) We observe the formation of a bimodal momentum distribution, meaning that only a fraction of the atoms gets accelerated by the pulse. **c**) From a 2D numerical simulation we indeed observe that the momentum distribution should develop a high-energy component, with a mean kinetic energy transferred by the speckle pulse $\Delta E_{kin} = 0.19(2)V_R$. **d**) The behavior we observe in the experiment is in agreement with the simulations. The evolution of E_{kin} of the excited part is approximately linear with V_R^{opt}, with a slope within 17% of the theoretical one. This confirms the validity of the optical calibration. The disorder strength reported in the paper is that obtained with the optical calibration, $V_R = V_R^{opt}$.

DOI: 10.1038/NPHYS3339

4. EXPANSION IN THE ANISOTROPIC DISORDER

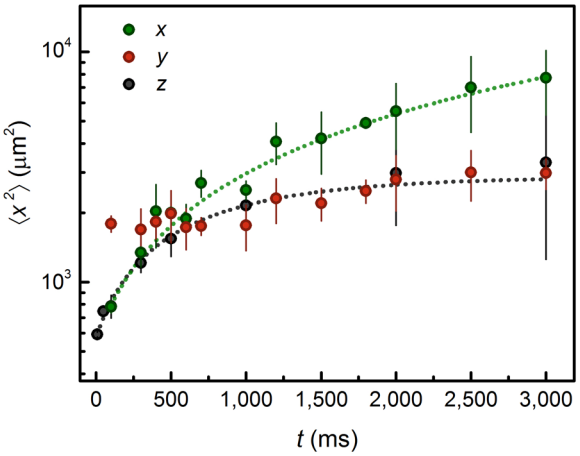

FIG. S4.

To estimate the effect of the anisotropic correlation function of the disorder, we look at the time evolution of the squared width of the spatial distribution $n(\mathbf{r})$ along the three main axes, for an intermediate value of the disorder amplitude V_R/k_B=23(2) nK. At short times the system expands along both x and z, eventually reaching a larger size along x, where the disorder correlation length is a factor $\sqrt{2}$ larger than along z. Along y we observe just a slight increase of $\langle y^2 \rangle$. This is consistent with the larger initial size, due to the anisotropy of the dipole trap, and the smaller correlation length caused by interference. In order to have the highest sensitivity to changes in the diffusion/localization dynamics, in our quantitative analysis we consider the evolution along x.

5. LOCALIZATION LENGTH

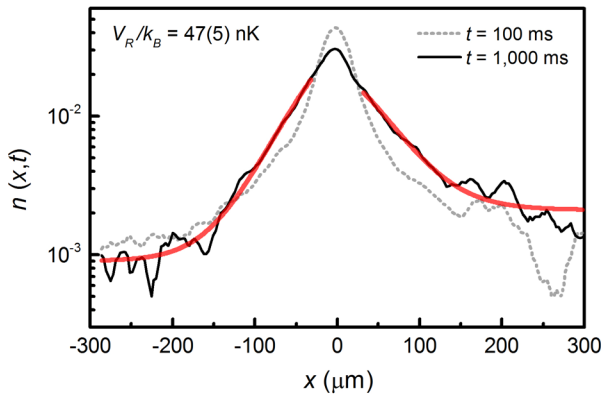

FIG. S5.

We estimate the order of magnitude of the localization length in our samples by fitting the tails of the in-situ density distribution after a long evolution time in the disordered potential. As a fitting function for the one-dimensional profiles we use $n(x) = 2\pi l^2 \Gamma(2, |x|/l)$, where $\Gamma(n, x)$ is the incomplete gamma function. It corresponds to the integral along two directions of a 3D exponential function with localization length l. We report here as an example the profile

for V_R/k_B=47(5) nK after 1 second of expansion in the disordered potential. Fitting the right and left tails of the distribution we obtain l_R=32(1)μm and l_L=28(1)μm. Note that this estimation might be affected by the presence of rather long tails even in the initial spatial distribution (see the profile at t=100 ms). We can compare these results with the predictions of the self-consistent theory in [3], which considers a similar disordered potential created by two interfering laser speckles. The localization length is predicted to change from about $l \sim \sigma_\perp$ around $E_c/3$ to $l \sim 100\sigma_\perp$ above $5/6E_c$, where $\sigma_\perp$ is the transverse correlation length of the individual speckle patterns. The localization lengths we measure correspond to $l \sim 30\sigma_\perp$, therefore of the right order of magnitude, since for this range of values of V_R we estimate to have a finite energy distribution close to E_c (see Fig.4b. in the main paper).

6. MOMENTUM DISTRIBUTION

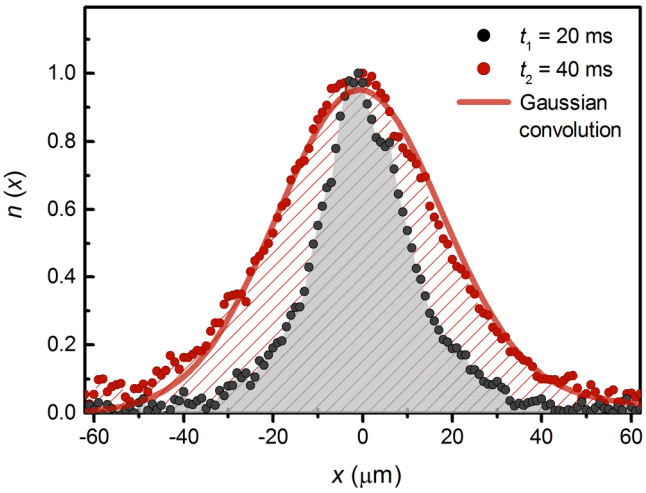

FIG. S6.

After loading the atoms into the disorder, we switch off the speckles and we measure the atomic density at two different times of flight, t_1 and t_2. We report here an example for V_R/k_B=47(5) nK. We then use a deconvolution procedure to deduce the momentum distribution. The spatial density at time t_2, integrated along y and z, is given by $n(x,t_2) = \int dk dx_1 n(x_1,t_1) n(k) \delta(x - x_1 - \frac{\hbar k}{m}(t_2 - t_1))$, where $k = k_x$ and $n(k)$ is the momentum distribution integrated along k_y and k_z. Here we have assumed the momentum and spatial distributions to be factorizable. The system indeed occupies a large number of states and we can reasonably assume that there are no relevant correlations in the average distributions. As shown in the figure, a Gaussian form of $n(k)$ well reproduces the data. We then substitute $n(k) \propto \exp(-k^2/(2\sigma^2))$ in the previous formula and we get $n(x,t_2) = \int dx_1 n(x_1,t_1) \exp\left[-\frac{1}{2}\left(\frac{m(x-x_1)}{\sigma(t_2-t_1)}\right)^2\right]$. We include the experimental $n(x_1,t_1)$ in the integral and we use it to fit the density distribution at time t_2, with σ as the only free parameter. From the value of $\sigma^2 = \langle k^2 \rangle$ we can calculate the mean kinetic energy as $E_{kin} = 3(\hbar^2 \langle k^2 \rangle / 2m)$, which for this dataset is 16.5 nK.

DOI: 10.1038/NPHYS3339

7. NUMERICAL STUDY OF LOW ENERGY EIGENSTATES

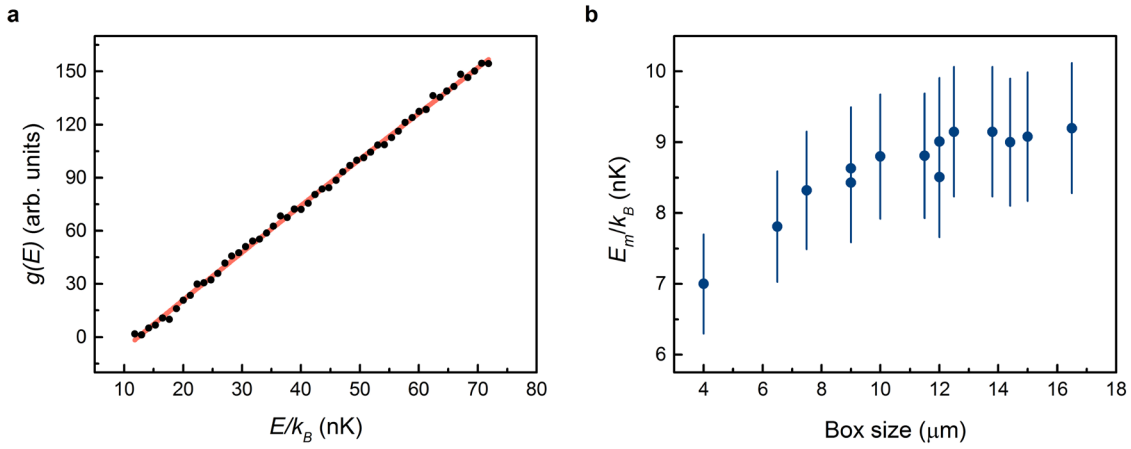

FIG. S7.

We solve the single-particle Schrödinger equation by exact diagonalization of small size systems. The Hamiltonian is $H = \mathbf{p}^2/(2m) + V_{speckle}(\mathbf{r})$, where $V_{speckle}$ is a 3D potential generated by the interference of two synthetic speckles with transverse correlation length $\pi\sigma_R$=2.4 μm, corresponding to the average of the experimental ones. We have neglected the longitudinal evolution of each speckle field, which is on a much larger lengthscale. The typical system is a cubic box with side length L=12.5 μm and a discretization length of 0.25 μm. The axes of the cube are along the three principal axes of the crossed speckle field. All results are averaged over at least 50 different realizations of the disorder.

From the i-th eigenfunction in real space $\psi(E_i, \mathbf{r})$ we evaluate by Fourier transform the momentum distribution, which we integrate along two spatial directions as in the experiment to get $|\psi(E_i, k)|^2$. The disorder-averaged collection of all $|\psi(E_i, k)|^2$ is, besides a normalization constant, the spectral function $\rho(E, k)$. The average density of states $g(E) = \int \rho(E, k)dk$ shows a power law scaling for energies larger than a certain minimum energy E_0: $g(E) \propto |E-E_0|^\alpha$. The typical exponents for $g(E)$ are between 1 and 2, and they grow with V_R: in the example reported in (**a**) for V_R/k_B=47 nK, we find $\alpha \simeq 1$. According to this scaling of $g(E)$, we use the function $n(E) = g(E)f(E) = (E - E_0)^\alpha \exp(-(E - E_0)/E_m)$ to fit the data of $n(E)$ obtained as in Fig.3 in the paper, where E_m was deduced in the reconstruction process (Fig.3a) while E_0 and α are free parameters.

To estimate finite-size effects, we have performed the simulations for various box sizes and then we have studied how the calculated quantities in momentum space evolve with the box size. In (**b**) we report for example E_m vs the box size for V_R/k_B=47nK and discretization lengths in the range (0.2-0.3) μm. For small sizes E_m shows a clear evolution with the size, while for larger sizes it tends to saturate. This indicates that boxes of (12-16)μm are large enough to correctly describe the evolution in momentum space of the eigenstates in the energy range of our interest. We note that if we perform a similar analysis in real space, for example by evaluating the one-dimensional participation ratio $1/\int(\int \psi(x, y, z)^2 dydz)^2 dx$, which is a measure of the characteristic length of the eigenfunctions, we find instead that our characteristic box of 12 μm gives reliable results in real space only up to energies of the order of $V_R/3$.

8. EXCITATION SPECTROSCOPY

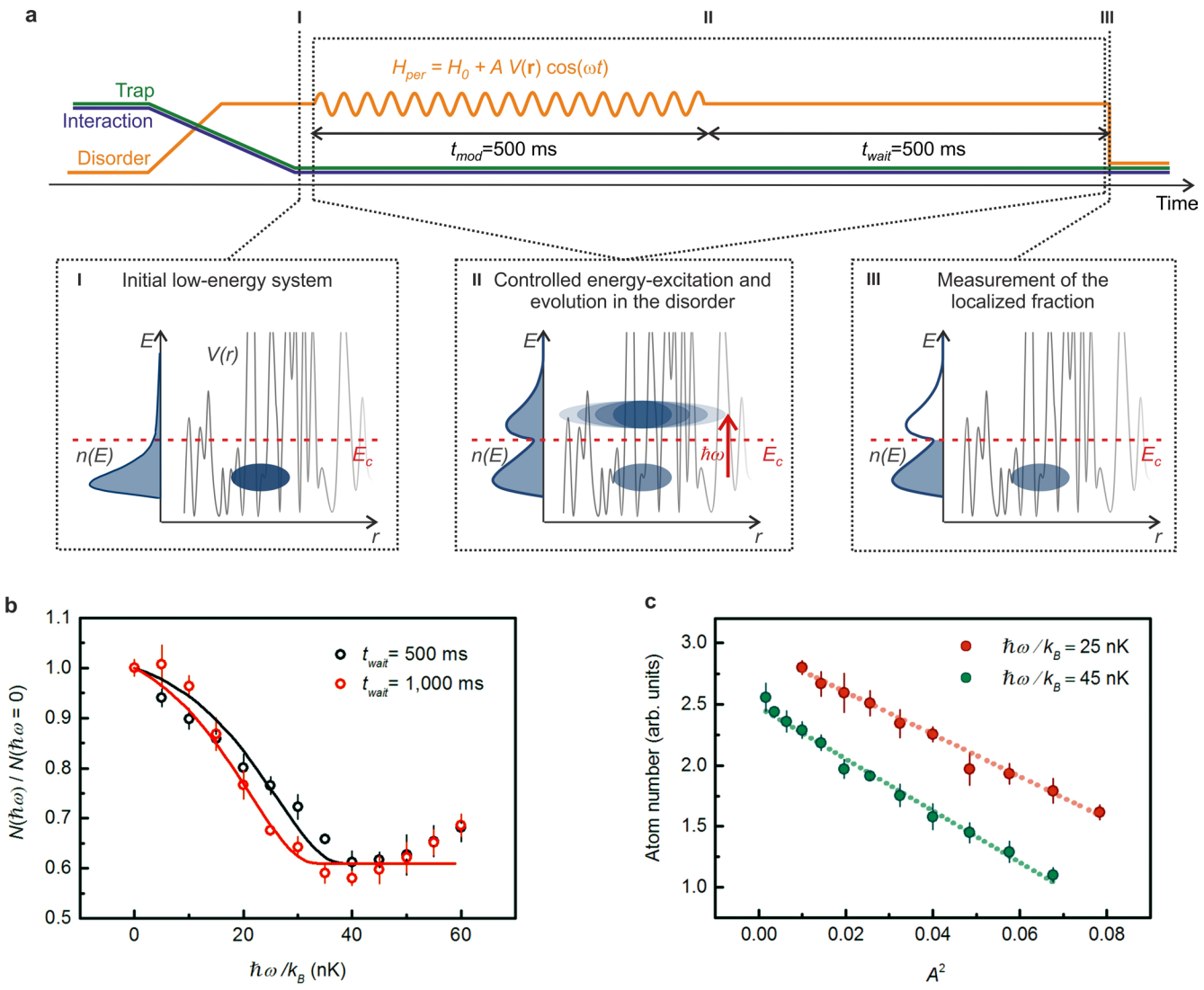

FIG. S8.

a) Scheme of the experimental sequence used to produce controlled excitations in the system. We choose the duration of the modulation and the successive waiting time ($t_{mod} + t_{wait}$=1 s) according to the fact that the diffusion coefficients from 0.5 s up to the largest times in Fig.2c are well below the diffusion quantum limit $\hbar/3m$. This means that the residual dynamics we observe in this time interval can be associated both to diffusive atoms very close in energy to the mobility edge and to localized atoms with long localization lengths that are still adapting to their equilibrium configuration. Also after the excitation process, we expect that if some diffusive component is still detectable on this timescale, it can only induce a small shift in the estimation of E_c. In order to quantify this possible systematic shift, we perform the test reported in (**b**), where we measure the loss spectrum at two different waiting times t_{wait} =0.5 s and 1 s, for t_{mod}=0.5 s and V_R/k_B=47(5) nK. Observing a small shift in the position of the minimum atom number, we decided to build a simple model to estimate the asymptotic value of E_c. We start from the hypothesis that we are overestimating the position of the mobility edge because of the presence of slow diffusive atoms that are still visible in the imaging field of view, as suggested by the shift to lower energy of the minimum for increasing t_{wait}. We suppose that the value of $E_c(t_{wait})$ measured after a finite waiting time is shifted with respect to the true value $E_c(t_{wait} \to \infty)$

DOI: 10.1038/NPHYS3339

by an amount that decreases exponentially with time: $E_c(t_{wait}) = E_c(t_{wait} \to \infty) + C\exp(-t_{wait}/\tau)$. We plug this into the expression of the localized fraction $N_{loc}(E_c(t_{wait}), \hbar\omega) = \int_0^{E_c(t_{wait})} n'(E, \hbar\omega)dE$ and we use this formula to perform a simultaneous fit of the two datasets in (**b**), with $E_c(t_{wait} \to \infty)$, τ and C as free parameters. The black and red lines in (**b**) represent the result of the fit at 0.5 s and 1 s respectively. We find $E_c(t_{wait} \to \infty)$=44(3) nK, C=0.5(1) nK and τ=0.3(1) s. This implies a shift of the mobility edge with respect to the one measured at t_{wait}=0.5 s of 6 nK. Since we cannot support the model for $E_c(t_{wait})$ with a complete set of data as a function of time, we think it is more appropriate to use this result as a systematic error rather than as a proper determination of the asymptotic value. A systematic error of -6 nK is then added to the statistical uncertainties in the measurements of E_c, resulting in the asymmetric error bars of Fig.5.

It is interesting to note that an analysis of the maximum size reached after the modulation (data in Fig.4**c** of the main paper), leads to the estimation of an effective diffusion coefficient for the system with the largest kinetic energy: $D = \Delta\langle x^2\rangle/2\Delta t \simeq \hbar/2m$. This value is of the same order of the one we measure for systems that have a peak energy close to the mobility edge from the very beginning (e.g. the data at V_R/k_B=23 nK in Fig.2**a**), confirming that the peak energy of the excited system after the modulation is close to the mobility edge.

Our model of the excitation process is built in the framework of the Fermi's golden rule. Given the perturbed Hamiltonian $H_{per} = H_0 + AV(\mathbf{r})\cos(\omega t)$, the excitation probability is $p(E,\omega) = A^2 \sum_{i,f} |\langle f|V(\mathbf{r})|i\rangle|^2 \delta(E_i - E)\delta(E_f - (E + \hbar\omega))$, where E is the initial energy and ω is the modulation frequency. To test the validity of this perturbative approach, we have verified that the atom number at the end of the excitation sequence, which is proportional to $1-p(E,\omega)$, scales linearly with A^2. See for example the measurements shown in (**c**) for two different values of ω for V_R/k_B=47(5) nK, which confirm that we are in the linear response regime.

Using numerical simulations, we estimate the dependence of the excitation probability p on the initial energy of the atom E, at least for low modulation frequencies (so as to stay in the low-energy regime where the simulations are reliable). We find a typical linear scaling $p(E) = p_0 + cE$ with $p_0 \simeq 0.5$ and $c \simeq 0.2$ nK^{-1}. If we consider this dependence in the calculations for $n'(E, \hbar\omega)$, we find only a small shift of E_c with respect to the one obtained for $p(E,\omega)$ =const. Actually, even a 3 times larger c than the one we get in the simulations would not change E_c by more than 2 nK. This very weak dependence on the actual form of p is due to the fact that it is mainly the low energy part of the spectrum, i.e. the steep increase of $n(E)$ between E_0 and E_p, that determines the shape of $N(\omega)$. We therefore conclude that the approximation $p(E,\omega)$ =const provides reliable results for the mobility edge.

[1] Landini, M. et al. Direct evaporative cooling of ^{39}K atoms to Bose-Einstein condensation. *Phys. Rev. A* **86**, 033421 (2012).
[2] Goodman, J. W. *Speckle phenomena in optics: theory and applications* (Roberts and Company Publishers, 2007).
[3] Piraud, M., Pezzé, L. & Sanchez-Palencia, L. Matter wave transport and Anderson localization in anisotropic three-dimensional disorder. *Eur. Phys. Lett.* **99**, 50003 (2012).